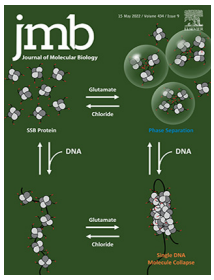

Structures of RGL1 RAS-Association Domain in Complex with KRAS and the Oncogenic G12V Mutant

Ben J. Eves [1], Teklab Gebregiworgis [1], Geneviève M. C. Gasmi-Seabrook [1], Douglas A. Kuntz [1], Gilbert G. Privé [1,2,3], Christopher B. Marshall [1] and Mitsuhiko Ikura [1,2*]

*1 - **Princess Margaret Cancer Centre,** University Health Network, Toronto, ON M5G 1L7, Canada*
*2 - **Department of Medical Biophysics,** University of Toronto, Toronto, ON M5G 1L7, Canada*
*3 - **Department of Biochemistry,** University of Toronto, Toronto, ON M5S 1A8, Canada*

Correspondence to Mitsuhiko Ikura: *Princess Margaret Cancer Centre, University Health Network, Toronto, ON M5G 1L7, Canada. Mitsu.Ikura@uhnresearch.ca (M. Ikura) @B_Eves (B.J. Eves), @CyclistDoug (D.A. Kuntz)*
https://doi.org/10.1016/j.jmb.2022.167527
Edited by C. Kalodimos

Abstract

Ral Guanine Nucleotide Dissociation Stimulator Like 1 (RGL1) is a RAS effector protein that activates Ral GTPase by stimulating nucleotide exchange. Most structures of RAS-effector complexes are for the HRAS isoform; relatively few KRAS-effector structures have been solved, even though KRAS mutations are more frequent in human cancers. We determined crystal structures of KRAS/RGL1-RAS-association (RA) domain complexes and characterized the interaction in solution using nuclear magnetic resonance spectroscopy, size-exclusion chromatography combined with multi-angle light scattering and biolayer interferometry. We report structures of wild-type KRAS and the oncogenic G12V mutant in complex with the RA domain of RGL1 at < 2 Å resolution. $KRAS^{WT}$/RGL1-RA crystallized as a 1:1 heterodimer, whilst $KRAS^{G12V}$/RGL1-RA crystallized as a heterotetrameric structure in which RGL1-RA dimerized via domain-swapping the C-terminal beta-strand. Solution data indicated that $KRAS^{WT}$ and $KRAS^{G12V}$ in complex with RGL1-RA both exist predominantly as 1:1 dimers, while tetramerization occurs through very slow association. Through detailed structural analyses, the distance and angle between RAS α1 helix and RBD/RA α1 helix were found to differ significantly among RAS and RBD/RA complexes. The KRAS/RGL1-RA structures possess some of the largest $\alpha1^{RAS}/\alpha1^{Effector}$ distances (21.7–22.2 Å), whereas the corresponding distances in previously reported RAS/RAF complexes are significantly shorter (15.2–17.7 Å). Contact map analysis identified unique structural signatures involving contacts between the β1-β2 loop of RA and the α1 helix of RAS, clearly distinguishing the KRAS/RGL1-RA (and other RAS/RA complexes) from RAS/RBD complexes. These results demonstrate that RAS effectors employ an assortment of finely-tuned docking surfaces to achieve optimal interactions with RAS.

Introduction

RAS genes are frequently mutated in cancer, with approximately 20% of all human cancers harboring a RAS mutation.[1] Of the three isoforms: HRAS, NRAS and KRAS, KRAS is the most frequently mutated and accounts for 75% of all RAS-mutant cancers.

The RAF/MEK/ERK and PI3K/AKT/mTOR pathways have been the main focus of RAS

signaling in oncogenesis; however, at least ten other RAS effector pathways have been identified.[2–3] Among these, the guanine nucleotide exchange factors of the RAS-like (Ral) small GTPases (RalGEFs) have emerged as important effectors of mutant RAS in pancreatic, colon, and other cancers, however, relative to RAF and PI3K, this pathway has not been as well characterized, especially in structural and mechanistic details of the RAS-RalGEF interactions.[4]

The first identified and most characterized RalGEF was RalGDS (Ral guanine nucleotide dissociation stimulator). In addition, three paralogues of RalGDS have been identified in mammals: RGL1 (RalGDS Like 1), RGL2, and RGL3, to comprise a RalGDS family of four proteins. The RalGDS family are multidomain proteins consisting of a RAS exchange motif (REM) domain at the N-terminus, a Cdc25-like GEF domain, and a RAS-association (RA) domain at the C-terminus (Figure 1(a)). RalGDS family proteins are recruited to the plasma membrane through interaction of their RA domain with active GTP-bound farnesylated RAS, shuttling these proteins from the cytosol to the plasma membrane. Ral GTPases are also located at the membrane, and the recruitment of RalGDS family proteins facilitates nucleotide exchange and conversion of Ral GTPases to the active GTP-bound form (Figure 1(b)). Additionally, the RA domain of RGL1 has been reported to interact with Tumor necrosis factor alpha induced protein 8-like 2 (TIPE2), a poorly understood anti-inflammatory protein with a unique helical structure. TIPE2 binding to the RA domain prevents binding of RAS and thereby inhibits the activation of downstream Ral signaling.[5] The Cdc25-like GEF domain of RalGDS shares $\sim$ 25% amino acid identity with other mammalian RAS-GEFs such as RAS guanine nucleotide releasing protein 1 (RASGRP1) and Son of Sevenless (SOS).[6] The REM domain regulates RalGDS activity through autoinhibition, by blocking the catalytic domain of RalGDS through intramolecular interactions. The RA-domains of the RalGDS family members and the RAS-binding domains (RBDs) of the Raf kinases share a ubiquitin-like conformation and contact the switch I region via a similar binding mode (formation of an antiparallel intermolecular beta-sheet).[7] Despite the structural similarities between RBDs and RAs, their sequence identity is very low.[8]

RAS has been shown to signal to RalB via RGL1 and RGL2, and promote invasion through the RAS-RGL1/2-RalB-exocyst-WRC pathway.[9] However, there is limited structural information available for RGL1 and the other RalGEFs. The only currently available structure of RGL1 is the solution structure of mouse RGL1-RA (residues 632–734), which when compared with the RalGDS-RA structure determined by X-ray crystallography, displayed a similar overall fold but differences in the loop regions, despite their high overall sequence homology.[10]

Although KRAS is the most commonly mutated RAS isoform, most structures of RAS complexes solved to date used the HRAS isoform.[11–12] HRAS has been commonly used as a model for the other RAS isoforms on the basis of their sequence similarity, but although the isoforms share 100% sequence identity in the N-terminus of the G domain (residues 1–86), residues 87–166 share only 82% sequence identity, and the C-terminal hypervariable region (HVR) (residues 165 to 184/185) are highly divergent with only 8% sequence identity, mainly found in the CaaX box prenylation motif.[13–14] Additionally, the three different RAS isoforms have been shown to be biochemically distinct and molecular dynamics simulations suggest that KRAS is the most flexible RAS isoform.[15–16]

Different RAS mutations have been shown to selectively activate specific effector pathways, with non-small cell lung cancers bearing KRAS G12C or G12V mutations exhibiting higher Ral GTPase activation and lower PI3K/AKT or RAF/MEK/ERK pathway activation compared to those with wild-type KRAS or other mutations.[17]

To gain more precise structural insight into the mechanisms of KRAS-mediated RGL1 regulation, we investigated the interaction of KRAS (WT and G12V) with RGL1 RA domain. We present crystal structures of KRAS (WT and G12V) bound to RGL1-RA. The structure of the $KRAS^{WT}$/RGL1-RA complex showed a 1:1 heterodimer as anticipated, whereas $KRAS^{G12V}$ crystallized as a symmetric 2:2 heterotetramer with RGL1-RA in the crystal. The two RGL1-RA molecules were connected by strand-swapping of β-5, and each RGL1-RA molecule interacts with both $KRAS^{G12V}$ molecules, one via the canonical binding interface found for other RAS effectors and one via a distinct secondary interface. We further studied the KRAS/RGL1-RA interaction in solution using biolayer interferometry (BLI), size exclusion chromatography combined with multi-angle light scattering (SEC-MALS), and nuclear magnetic resonance (NMR) spectroscopy. These solution experiments suggested both wild-type and G12V complexes exist primarily as 1:1 complexes, but the observation of multiple cross-peaks in the ^{1}H-^{15}N heteronuclear single quantum coherence (HSQC) spectra indicate the presence of multiple conformational states, which might include a very low population of 2:2 KRAS/RGL1-RA complexes. Furthermore, a species with molecular weight consistent with that of the 2:2 KRAS/RGL1-RA complex was observed when SEC-MALS experiments were repeated with samples that had been stored for 6 months. A detailed comparison was performed between the structures of the KRAS/RGL1-RA complexes and all previously reported KRAS/HRAS complexes with the RA/RBDs of other effector proteins.

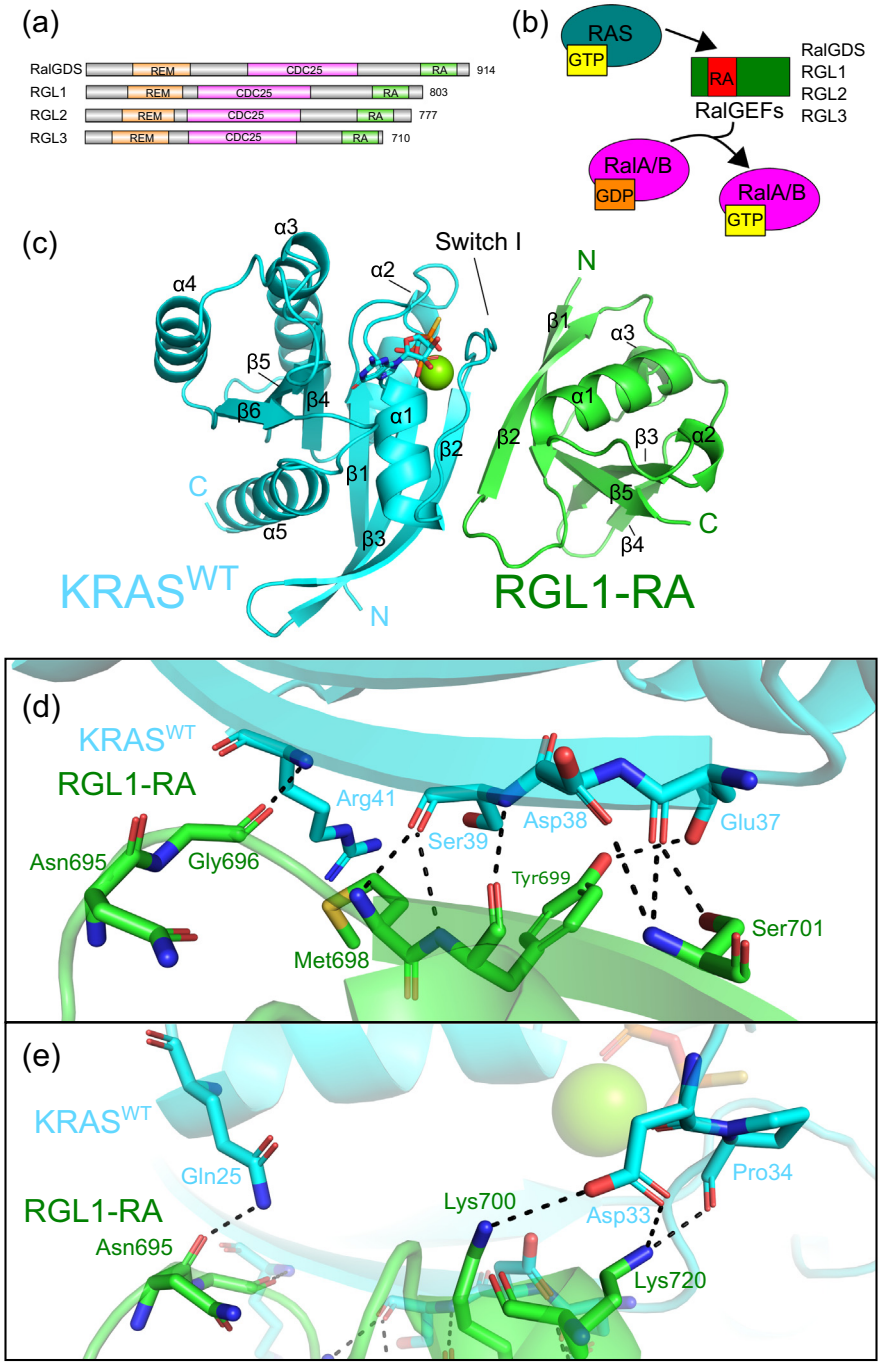

Figure 1. RalGDS family and the structure of the KRAS^{WT}/RGL1-RA complex. (a) RalGDS family domain structure (Figure produced using DOG[22]). (b) RalGDS family as regulators of Ral**.** (c) Crystal structure of KRAS^{WT}/RGL1-RA complex shown in cartoon representation. KRAS^{WT} is colored cyan, and RGL1-RA is colored green. GTPγS is shown as sticks and Mg^{2+} is shown as a green sphere. Enlarged view of the KRAS^{WT}/RGL1-RA interface interactions formed by β2 strand (d) and the switch I region (e) of KRAS^{WT}. Residues involved in the binding interface are shown in stick representation and contacts between these residues are illustrated by dashed black lines.

Results

Crystal structure of wild-type full-length KRAS bound to RGL1-RA

We first investigated the structure of human KRAS4B^{WT} (residues 1–185, C118S, lacking farnesylation and methylation of C185 at the C-terminus) in complex with the hydrolysis-resistant GTP analogue guanosine 5′-O-[gamma-thio]tripho sphate (GTPγS) and human RGL1-RA (residues 681–773). KRAS4B^{WT} was expressed as an N-terminally His-tagged protein and RGL1-RA as a

GST fusion protein in *Escherichia coli* (BL21 DE3 Codon+) and the tags were removed during purification. The two purified proteins were mixed immediately prior to crystallization screening and the $KRAS^{WT}$/RGL1-RA complex crystallized in 0.05 M Magnesium acetate tetrahydrate, 0.1 M MES (pH 6.5), 26% v/v PEG 400. Several commercial sparse-matrix crystallization screens were employed but only the MemGold2 (Molecular Dimensions) screen produced diffraction-quality crystals. Crystals collected from the screening condition without further optimization diffracted to a resolution of 1.96 Å at the Brookhaven synchrotron light source, and the crystal structure was solved by molecular replacement using a structure of a HRAS/RalGDS-RA complex (PDB code 1LFD) as the search model.[18] The structure was solved with one $KRAS^{WT}$ and one RGL1-RA per asymmetric unit, with space group P 63 2 2. Data collection and refinement statistics for each complex can be found in Table S1.

The asymmetric unit of the structure consists of one unit of $KRAS^{WT}$ (1–185) bound to one GTPγS molecule, and one magnesium ion, complexed to one unit of RGL1-RA (681–773) (Figure 1(c)). Clear, continuous electron density was observed for all residues in the maps, with the exception of the N- and C-terminal residues of RGL1-RA (681–682, and 769–773, respectively), and the flexible C-terminal hypervariable-region of $KRAS^{WT}$ comprising residues 170–185.

Not surprisingly, the RGL1-RA shares the same ubiquitin-like fold with the RA of RalGDS and the RBD of RAF.[19–20] $KRAS^{WT}$ and RGL1-RA interact along the outer strands of their respective β-sheets (i.e., β-strand 2 in $KRAS^{WT}$ and β-strand 2 in RGL1-RA) to form an extended intermolecular β-sheet between the two proteins. $KRAS^{WT}$ residues Gln-25, Asp-33, Pro-34, Glu-37, Asp-38, Ser-39 and Arg-41 of switch I comprise the binding interface, along with RGL1-RA residues Asn-695, Gly-696, Met-698, Tyr-699, Lys-700, Ser-701 (in β-strand 2) and Lys-720 (in α-helix 1), as shown schematically in Figure 2. The residues involved in the KRAS/RGL1-RA interface are structurally homologous to the canonical interface found in the HRAS/RalGDS-RA and HRAS/RAF-RBD complexes, with the interaction between the β-strands in an extended β-sheet conformation providing the major binding site (Figure 1(c), (d)).[18,21]

Crystal structure of full-length $KRAS^{G12V}$ bound to RGL1-RA

Based on our previous finding that G12V mutation enhanced the affinity of HRAS for RGL1, we sought to determine whether this mutation alters the interface of the KRAS/RGL1 complex by pursuing the structure of GTPγS-loaded $KRAS4B^{G12V}$ (1–185, G12V/C118S) bound to RGL1-RA. $KRAS^{G12V}$ and RGL1-RA were purified and mixed in a 1:1 ratio. This complex did not crystallize in the same condition as $KRAS^{WT}$, however, it was successfully crystallized in a distinct condition (0.1 M BIS-TRIS (pH 5.5), 25% w/v PEG 3350). Although both complexes produced crystals in several different conditions, there was no overlap, i.e., there was no single condition in which both complexes crystallized, suggesting the mutation may alter the overall structure and thus the crystal contacts. A crystal collected from the screen (Index HT, Hampton Research) without further optimization diffracted to a resolution of 1.98 Å at the Advanced Photon Source synchrotron (Argonne National Laboratory, Argonne, IL). The crystal structure of the mutant complex was solved using the same molecular replacement search model as for wild type,[18] but with the distinct space group C 1 2 1. Data collection and refinement statistics can be found in Table S1. The electron density was clear and continuous for all residues except the RGL1-RA termini (same as the WT complex), and the $KRAS^{G12V}$ HVR (residues 170–185).

The structure of the $KRAS^{G12V}$ mutant bound to RGL1-RA appeared similar to the wild-type complex, however, during refinement it became apparent that the quaternary structure was different. The electron density in the loop region between α-helix 3 and β-strand 5 was not continuous in the replacement model, however rebuilding this region revealed a structure in which β-strand 5 was unfolded (SI Figure 1), which was then used to search for the quaternary structure. In contrast to the 1:1 complex structure of $KRAS^{WT}$ bound to RGL1-RA, the crystal structure of the $KRAS^{G12V}$ complexed with the same RA domain revealed a heterotetrameric assembly consisting of two symmetric $KRAS^{G12V}$/RGL1-RA heterodimers, each comprising one unit of $KRAS^{G12V}$ (1–185) bound to one GTPγS molecule, and one magnesium ion, complexed to one unit of RGL1-RA (681–773) (SI Figure 2(a)). Within the tetrameric assembly, the C-terminal β-strand of each RGL1-RA was domain-swapped with the RGL1-RA of the other protomer in a symmetrical manner. The β5-strand of each RGL1-RA detached from the position observed in the $KRAS^{WT}$/RGL1-RA complex and inserted into the equivalent position in the other $KRAS^{G12V}$/RGL1-RA dimer. To accommodate this domain-swapping transition, the loop connecting the β5-strand to the α3-helix of RGL1-RA opens into an extended conformation.

The canonical binding interface between each $KRAS^{G12V}$ switch I region and RGL1-RA is very similar to that of the $KRAS^{WT}$/RGL1-RA complex as described in the previous section, although the domain-swapping results in some slight differences. In addition to the interacting residues observed in the WT complex ($KRAS^{G12V}$ residues Gln-25, Asp-33, Pro-34, Glu-37, Asp-38, Ser-39 and Arg-41, along with RGL1-RA residues Asn-695, Gly-696, Met-698, Tyr-699, Ser-701 and

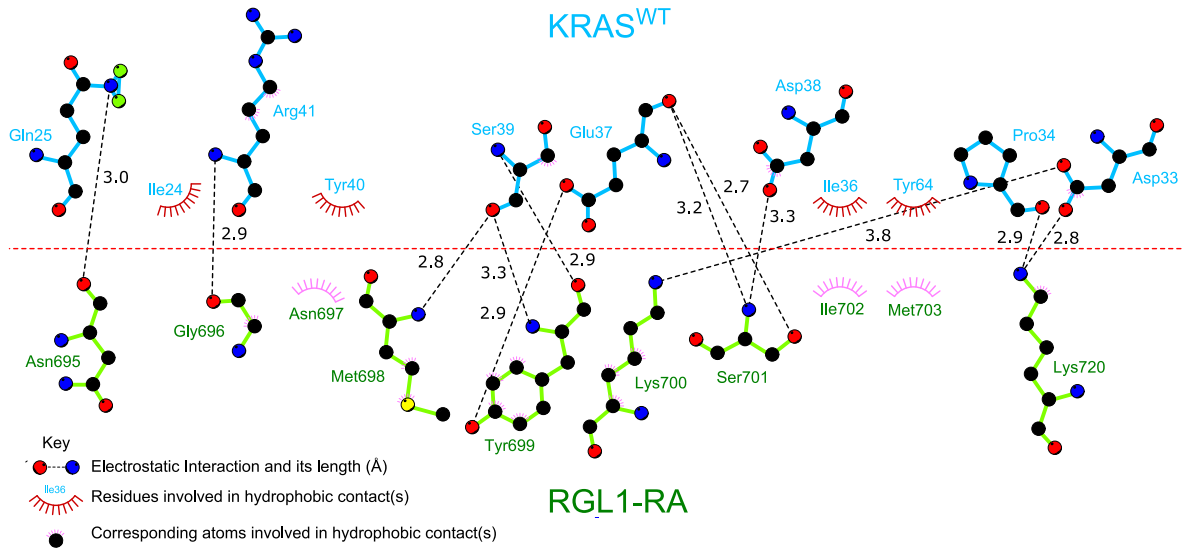

Figure 2. Schematic diagram showing contacts of the KRAS^{WT}/RGL1-RA complex binding interface. Black dashed lines indicate electrostatic interactions with their distances (Å). The horizontal red dashed line represents the protein–protein interface. RGL1-RA residues Asn-695, Gly-696, Met-698, Tyr-699, Lys-700, Ser-701 are in β-strand 2 while Lys-720 is in α-helix 1.

Lys-720), reorganization of the contacts between β-strand 1 and the domain-swapped β5 strand of RGL1-RA allows Arg688 of β-strand 1 to form an additional interaction with Glu37 of KRAS^{G12V}, increasing the number of contacts in the extended intermolecular β-sheet (Figure 3).

In addition to the canonical binding interface observed in both the KRAS^{WT}/RGL1-RA and KRAS^{G12V}/RGL1-RA structures, a second interface was observed between each protomer within the heterotetrameric assembly in the KRAS^{G12V}/RGL1-RA crystal. These contacts form between KRAS^{G12V} of one protomer and RGL1-RA of the other protomer involving RGL1-RA residues Asp740, Lys741 (found between β-strand 3 and β-strand 4), and Ser757 (found between α-helix 1 and β-strand 4), located on the opposite face to the canonical binding interface. On the KRAS^{G12V} side, residues Lys5 (β-strand 1), Arg41 (Switch I region), Asp54 (β-strand 3), and Gln70 (Switch II region/ α-helix 2) contribute to these contacts (SI Figure 2(b)-(d) and Figure 3). This interface is highly electrostatic in nature, and encompasses a relatively small buried surface area (901 Å^2), typical of crystallization-induced contacts, while the domain-swapped interface involves an extensive network of hydrogen bonds and a much larger surface of 3875 Å^2. We further characterized this mutant complex to investigate whether the heterotetramer observed in the crystal is present in solution.

Comparison of RAS/effector complex structures

The RAS interacting domains of RAS effectors share weak amino acid sequence homology and historically have been classified, on the basis of sequence, as RAS binding domain (RBD) or RAS association domain (RA), although structurally both possess a highly similar α/β topology with some minor differences.[23] To better understand our structures of the KRAS/RGL1-RA complex and the structural differences between the complexation of RBDs and RAs to RAS, structures of the KRAS/RGL1-RA complexes were carefully compared to currently available complexes of RAS isoforms with the RA/RBDs of other effector proteins. We first noticed significant differences in the location of the α1 helices of the RBD/RAs (up to 4 Å) among all RAS/RBD-RA complexes when the RAS molecules in each complex were superimposed. Hence, we chose to measure the distances and angles between the α1 helix of RAS and the α1 helix of the effector in each complex (Table S2, Figure 4). Interestingly, a distinct separation between RBDs and RAs was observed (Figure 4), with some intermediates which will be discussed below. The general trend was that RAs exhibit a greater distance and angle between their α1 helices and RAS α1, compared to the RBDs. The average distance between these two α1 helices is 17.0 Å for RAS/RBDs and 21.2 Å for RAS/RAs. Most notably, KRAS/RA complexes with RalGDS-family effectors cluster in a region with the largest distances among all RAS/RA structures, including our KRAS/RGL1-RA complexes (21.7 Å for KRAS^{WT}/RGL1, 22.2 Å for KRAS^{G12V}/RGL1). In contrast, the RAS/RAF-RBD complexes form another cluster with significantly closer contacts between RAS α1 and RBD α1 (16.6 Å). In parallel with these variations in the $\alpha1^{RAS}/\alpha1^{Effector}$ distance, RA domains tend to have a straight α1 helix whereas the α1 helices of the RBDs curve and shift towards the α1 helix of RAS,

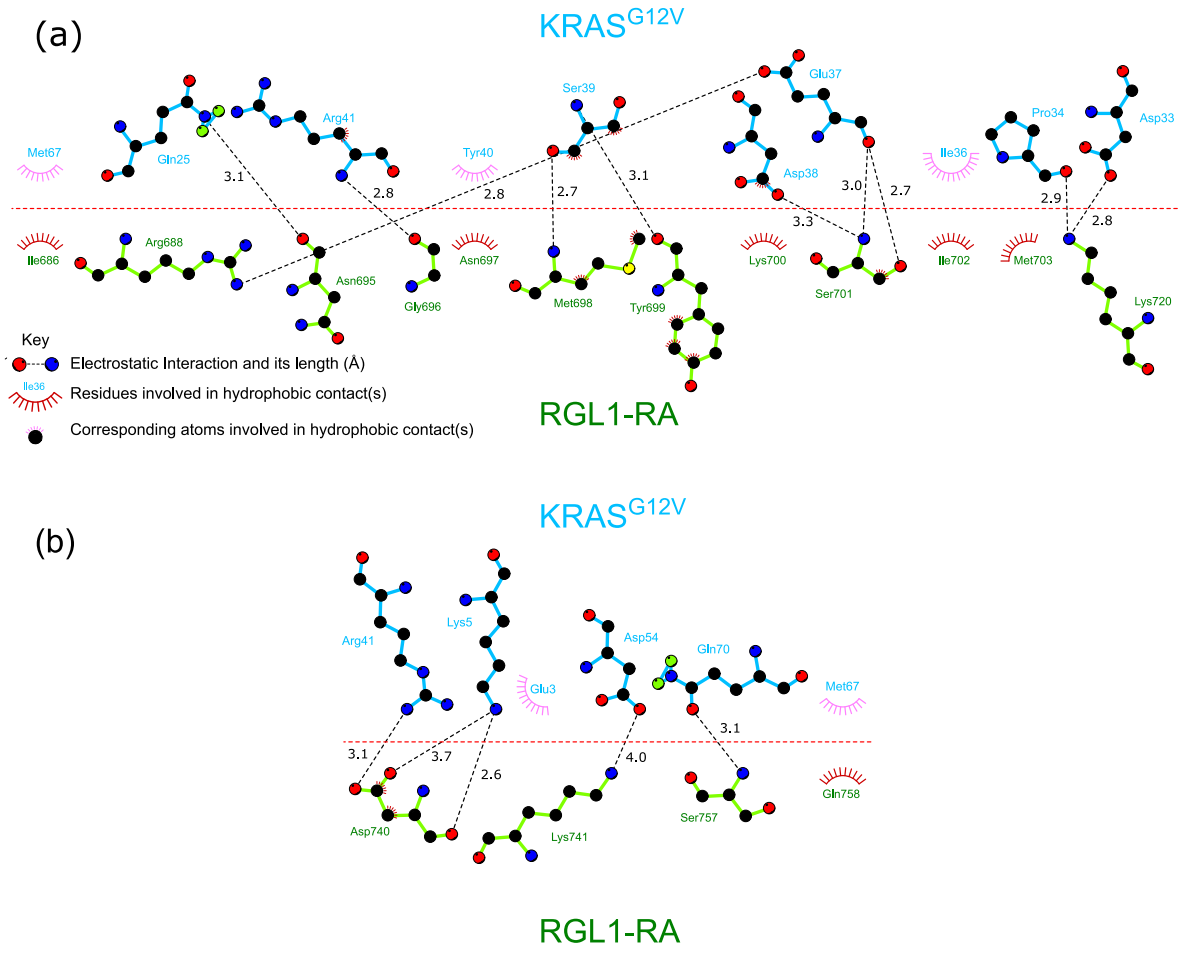

Figure 3. Schematic diagram showing contacts of the KRAS^{G12V}/RGL1-RA complex. (a) Schematic diagram of the canonical binding interface and (b) the secondary interface**.** Black dashed lines indicate electrostatic interactions with the distance (Å). The horizontal red dashed line represents the protein–protein interface.

facilitating additional contacts with both the α1 and Switch I regions of RAS (Figure 4). These analyses clearly indicate that the $\alpha1^{RAS}/\alpha1^{Effector}$ distance and angle between RAS and RBD/RA are excellent structural parameters to classify RAS/effector interactions and that RAS effectors use a wide range of finely-tuned docking surfaces to achieve optimal interactions with RAS.

Our $\alpha1^{RAS}/\alpha1^{Effector}$ distance and angle analyses identified five intermediates with features that fall between the two major structural groups: two RBDs and three RAs. HRAS Byr2-RBD is an intermediate with an α1 helix that curves towards the RAS α1 helix, as expected for an RBD, but the helix positioning is more similar to the RA domains. In the HRAS(G12V) PI3Kγ(V223K/V326A)-RBD structure the majority of the α1 helix is angled away from the RAS α1 helix, but this is followed by a second short α-helix angled towards the RAS α1/Switch I region. This is one of the few crystal structures that includes a full-length effector (PI3Kγ), thus the interactions with other domains may be distorting the α1 helix. In two of the RA outliers, HRAS Afadin-RA and HRAS (D30E/E31K) RASSF5(L285M/K302D)-RA, the effector α1 helix extends closer to the α1/Switch I region of RAS, resembling the RBD α1 helices. Finally, HRAS(G12V) PLCε(Y2176L)-RA $\alpha1^{RAS}$-$\alpha1^{Effector}$ helices have a greater angle than the main cluster observed for the RAs.

To further characterize the RAS interactions with effector RBD/RA domains, we analyzed the protein contact maps of the complexes to identify differences between RAs and RBDs. Distances between alpha carbons between pairs of RAS and effector residues within each complex were measured and those distances less than 12 Å were plotted by residue number (SI Figures 3–5). Distinct features were observed, which clearly separate the structures into two groups with some intermediates (Figure 5). The RBD group share two features: (i) presence of extensive contacts between the α1 helix of the effector and the α1 helix/switch I region of RAS; (ii) close proximity of

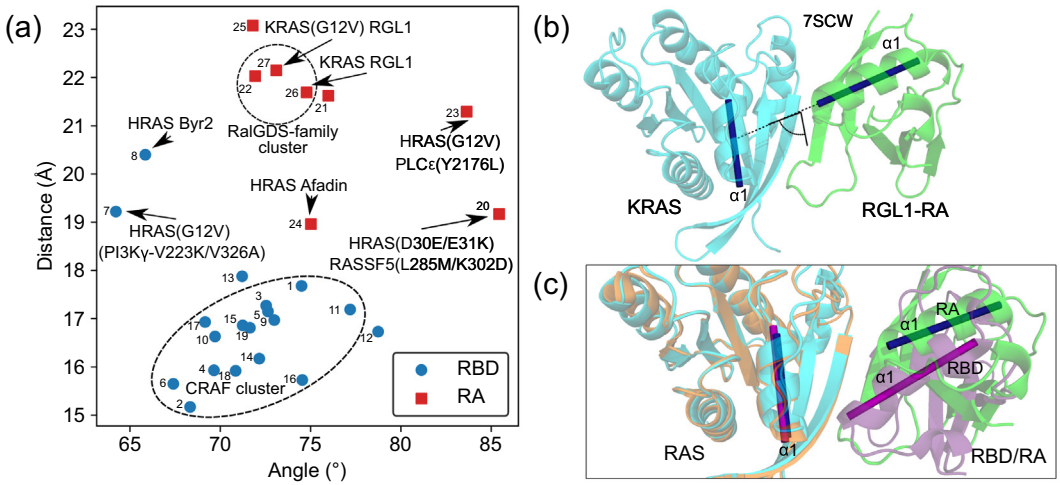

Figure 4. Distance and angle measurements between the α1 helix of RAS and α1 helices of RBD/RA effector complexes. (a) Comparison of distance and angle measurements. RBDs and RAs are shown as blue circles and red squares, respectively. KRAS/RGL1-RA complexes are highlighted as well as intermediates. Numbering scheme is shown in Table S2. (b) Depiction of distance and angle measurements between α1 helices of RAS and effectors within the complex. Distances were measured between the midpoint of the helices as depicted by the dashed line between cylinders. (c) Comparison of distance and angle between α1 helices of KRAS/RGL1(RA) (Cyan/Green) and HRAS/CRAF(A85K)(RBD)(Orange/Purple) depicted by blue and purple cylinders, respectively.

the loop region between β1 and β2 of the effector and the β2 strand of RAS. In contrast, the RA group possesses a unique feature involving intimate proximity of the loop region between β1 and β2 of the effector to the α1 helix of RAS (SI Figure 6). Indeed, our new structures of KRAS/RGL1-RA complex in both WT-KRAS and KRAS (G12V) possess this unique RA-type contact (Figure 5(a)) and lacks the RBD-specific features described above.

Our contact map analysis identifies some effectors with intermediate properties that diverge from the RA/RBD trends described above. While Afadin has been classified as an RA domain based on sequence, its structure in complex with HRAS (6AMB) exhibits RBD-like contacts. Likewise, GRAB14-RA/PH (K272A/E273A) in complex with HRAS(G12V) (4 K81) also exhibits more RBD-like contacts, whereas PLCε(Y2176L)-RA in complex with HRAS(G12V) (2C5L) exhibits a mixture of RBD and RA features. Byr2-RBD in complex with HRAS (1K8R) did not exhibit the characteristic α1 helix proximity to the α1 helix/switch I region of RAS generally displayed in RAS-RBD complexes. These intermediates observed by the contact map analysis overlap with those observed in the analyses of the RAS-RBD/RA α1-α1 positioning. The results may suggest

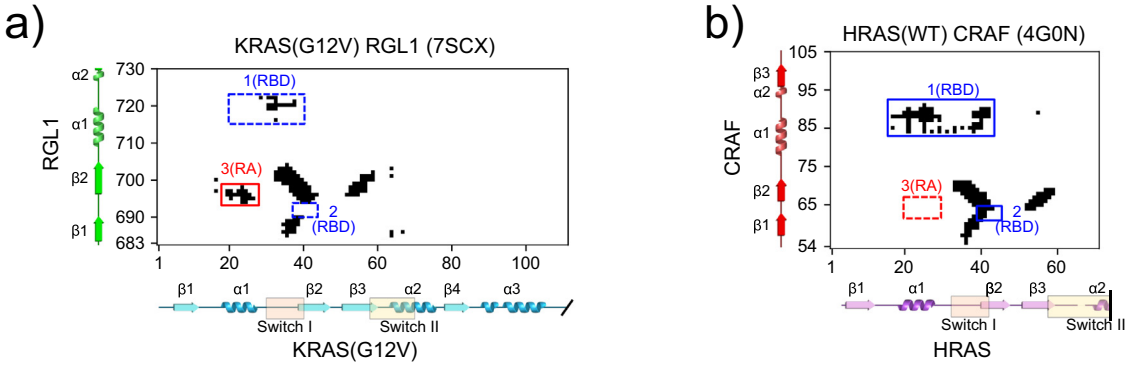

Figure 5. Contact maps of RAS/effector complexes. (a) Contact map of KRAS(G12V)/RGL1. (b) Contact map of HRAS/CRAF. Contacts are highlighted in black. RBD and RA unique features are enclosed by blue and red rectangles, respectively. Dashed rectangles depict the absence of a feature. Secondary structures are shown beside each axis and Switch I/II regions are highlighted for RAS. The additional contacts observed in the KRAS(G12V)/RGL1 heterotetrameric assembly in the crystal are shown in SI Figure 5.

that the current RA/RBD classification could be further separated into subclasses on the basis of structure.

Multiple conformational states of KRAS/RGL1 complexes in solution

To assess whether or not the KRAS(G12V)/RGL1-RAS complex exists as a tetramer in solution and also if the tetramerization is mutant specific, we employed NMR spectroscopy as well as size-exclusion chromatography combined with multi-angle light scattering (SEC-MALS). In the NMR experiments, we assigned the backbone resonances of RGL1-RA using three-dimensional (3D) backbone triple-resonance experiments to enable a comparison of the binding modes of $KRAS^{WT}$ and $KRAS^{G12V}$ with RGL1-RA in solution.[24] The ^{1}H-^{15}N HSQC spectrum of uniformly ^{15}N-labelled RGL1-RA, with assignments, is shown in SI Figure 7.

Upon addition of $KRAS^{G12V}$ or $KRAS^{WT}$, more than half of the ^{15}N-RGL1-RA resonances were broadened beyond detection (SI Figure 8). The

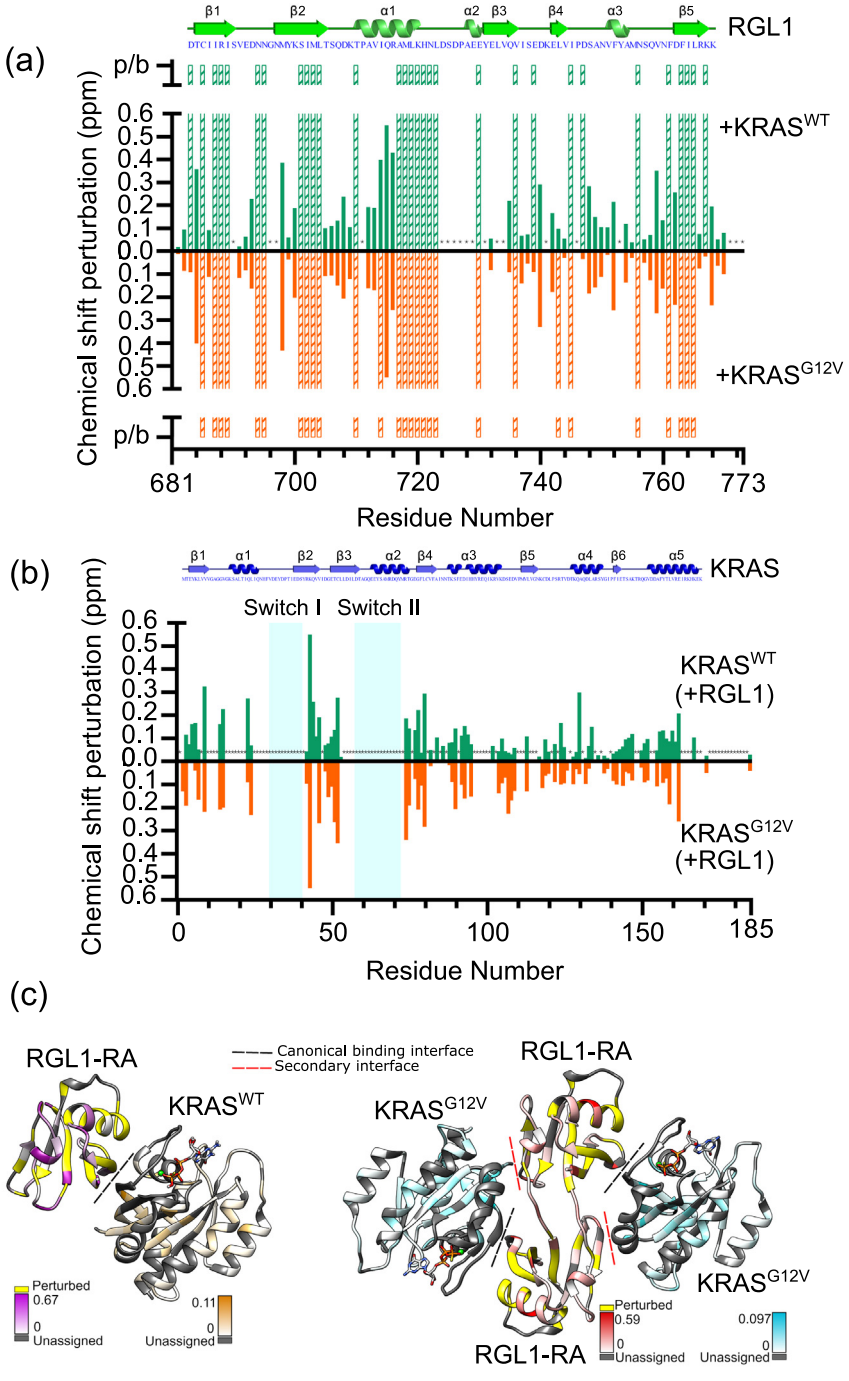

peak broadening patterns of ^{15}N-RGL1-RA induced by KRAS^{WT} versus KRAS^{G12V} were very similar overall, although small subsets of peaks were more severely broadened by one or the other form of KRAS. The chemical shift perturbations (CSPs) were plotted by residue number (Figure 6(a)) and mapped onto the complex crystal structures (Figure 6(c)). In both cases, the broadening was observed across the RGL1-RA domain and was not clearly localized to any specific region.

We also performed the complementary experiments by adding unlabeled RGL1-RA to ^{15}N-KRAS^{WT} or ^{15}N-KRAS^{G12V} (SI Figure 9). The resulting KRAS CSPs, which were similar overall for WT and G12V (Figure 6(b)), were also mapped onto the complex crystal structures (Figure 6(c)). Substantial CSPs are present at the sites of the secondary crystal contacts seen for KRAS^{G12V}/RGL1-RA (SI Figure 10). Due to the dynamics of KRAS in the GTPγS-bound form, the Switch II region is mainly unassigned, but some neighboring residues in this region as well as the interacting RGL1-RA residues exhibit strong chemical shift perturbations. Additionally, the β5-strand of RGL1-RA, which is domain-swapped in the crystal, is extensively perturbed upon addition of KRAS. While these CSPs are consistent with the existence of heterotetramization and domain-swapping in solution, they cannot be distinguished from CSPs induced by allosteric structural or dynamical changes induced by the canonical KRAS/RGL1-RA interaction. Indeed, the CSPs in both proteins extended well beyond the canonical interface and crystal contact sites. Additionally, to compare these binding events to other RAS effectors, we also investigated ARAF-RBD binding to ^{15}N-KRAS^{WT} or ^{15}N-KRAS^{G12V}.

The spectra of ^{15}N-KRAS^{G12V} or ^{15}N-KRAS^{WT} bound to RGL1-RA both exhibited several cases of peak splitting (Figure 7), suggesting that multiple KRAS residues exist in more than one conformational state in both WT and mutant ^{15}N-KRAS/RGL1-RA complexes. This peak splitting phenomenon was not apparent in the spectrum of ^{15}N-KRAS in complex with ARAF-RBD (SI Figure 11), suggesting multiple conformational states are a distinct feature of the KRAS/RGL1-RA complexes. Although the crystal structures captured the KRAS^{G12V}/RGL1-RA complex in a heterotetrameric state whereas the KRAS^{WT}/RGL1-RA complex was heterodimeric, the NMR data suggests there is not a substantial difference between the two complexes in solution.

To more directly probe the stoichiometry of the KRAS/RGL1-RA complexes, we performed size-exclusion chromatography combined with multi-angle light scattering (SEC-MALS) experiments. The SEC-MALS chromatograms detected heterodimers, but not heterotetramers for both the wild-type and the G12V mutant complexes (SI Figure 12(a)). KRAS (1–185) has a MW of approximately 21.4 kDa whilst RGL1-RA has a MW of approximately 10.7 kDa, thus a heterodimer should exhibit a MW of $\sim$ 32 kDa and the MW of a heterotetramer should be $\sim$ 64 kDa. Neither the wild-type nor G12V complex produced a $\sim$ 64 kDa peak, rather both complexes exhibited similar $\sim$ 31 kDa peaks, suggesting that a 1:1 heterodimer is the major species in solution for both complexes. Some studies of domain-swapped dimers reports have reported very slow rates of monomer/dimer equilibration, with time-scales of months.[26–28] While this manuscript was in revision, we recovered the 6-month old NMR samples of ^{15}N-KRAS in complex with RGL1-RA. KRAS-GDP was detected as the major species in HSQC spectra, consistent with slow hydrolysis of GTPγS. Analysis of these samples by SEC produced chromatograms with a major peak corresponding to the elution positions of KRAS and RGL1-RA alone (consistent with dissociation of the complex upon GTPγS hydrolysis), as well as a smaller peak in the position of a KRAS:RGL1-RA heterodimer, and a new peak that eluted with an

Figure 6. Chemical shift perturbations induced by the KRAS/RGL1-RA interactions. (a) Chemical shift perturbations of RGL1-RA induced by binding of KRAS^{WT} or KRAS^{G12V}. RGL1-RA chemical shift perturbations induced by KRAS^{G12V} are shown in orange whereas changes induced by KRAS^{WT} are shown in green. Resonances detected in RGL1-RA but not in the complexes, due to large perturbations or severe peak broadening are shown as dashed bars with an arbitrary value (p/b, perturbed/broadened). Residues not assigned for RGL1-RA are marked with X. RGL1-RA secondary structure and sequence is depicted above the plot.[25] (b) Chemical shift perturbations of KRAS^{WT} or KRAS^{G12V} induced by binding of RGL1-RA. KRAS^{G12V}/RGL1-RA chemical shift perturbations are shown as negative values to compare changes to KRAS^{WT}/RGL1-RA. Residues not assigned for KRAS are marked with X. KRAS^{WT} secondary structure and sequence is depicted above the plot. (c) Chemical shift perturbations induced by the KRAS/RGL1-RA interactions mapped onto their crystal structures. KRAS^{WT} (left) or KRAS^{G12V} (right) complexes with RGL1-RA are shown with color intensity representing increasing magnitude of chemical shift perturbations induced by addition of the binding partner in each case (as defined by the scales shown). Resonances that were highly perturbed or broadened are shown in yellow. Residues without assignments are colored grey. White residues were unperturbed. Canonical binding interface and secondary interfaces are depicted as dashed lines, black and red respectively.

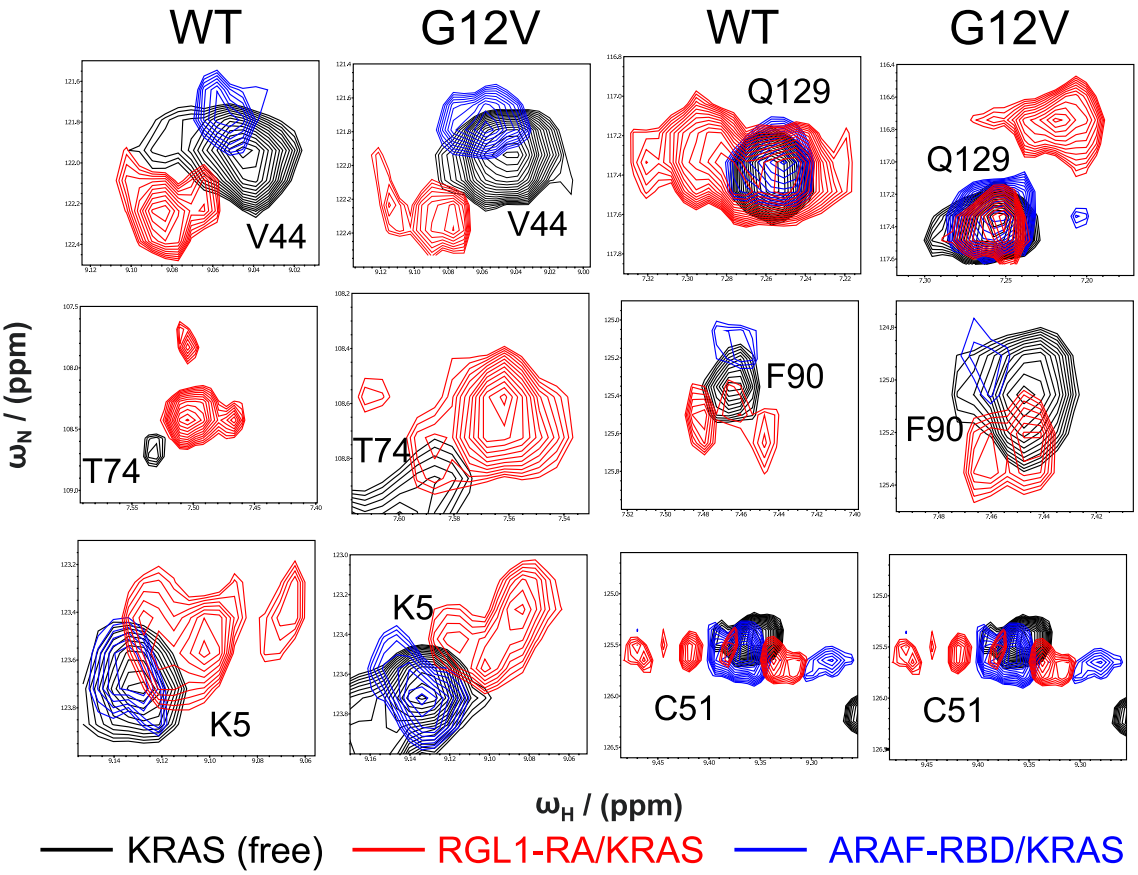

Figure 7. Multiple conformational states observed for KRAS bound to RGL1-RA. Overlaid spectra of ^{15}N-KRAS^{G12V} (left) and ^{15}N-KRAS^{WT} (right) alone (black), and in the presence of RGL1-RA (red) or ARAF-RBD (blue). In the presence of RGL1-RA, several split peaks were observed, suggesting KRAS exists in multiple conformational states when bound to RGL1-RA.

apparent molecular weight consistent with that of the heterotetramer observed in the KRAS G12V mutant complex (SI Figure 12(b)). Both WT KRAS and the G12V mutant produced similar dimer:tetramer ratios of ~ 1.75:1 and their low abundance is consistent with the lack of KRAS NMR signals from heterodimers/tetramers in this old sample. Considering the crystal structures, NMR and SEC-MALS results together, we propose that both the WT and mutant complexes can transition from 1:1 to 2:2 KRAS:RGL1-RA complexes, however the population of heterotetramer is extremely low and the transition from the dimer to the tetramer is a very slow process in solution.

Biolayer interferometry study of the KRAS/RGL1-RA complex

We also sought to determine whether the binding affinity of RGL1-RA for KRAS may change if the mutant induces tetramerization. In our previous studies, we determined using isothermal titration calorimetry (ITC) that HRAS^{G12V} mutation alters effector preference, in which HRAS^{G12V} displayed enhanced binding to RGL1 relative to ARAF, whereas HRAS^{WT} binds ARAF slightly better than RGL1.[3] In this study, we employed biolayer interferometry and immobilized GST-RGL1-RA fusion proteins on biosensors coated with anti-GST antibody (Pall FortéBio). Freshly prepared samples were used for these experiments. Analysis of the binding kinetics determined a dissociation constant (K_d) for KRAS^{WT} binding to RGL1-RA of 3.4 μM, whilst KRAS^{G12V} bound with a K_d value of 3.2 μM Figure 8. Steady-state data analysis produced remarkably similar K_d values (K_d 3.7 μM and 3.4 μM, respectively). Thus, the anticipated enhanced binding of KRAS^{G12V} to RGL1-RA compared to that of KRAS^{WT} was not considered significant. These results are in full agreement with the aforementioned NMR and SEC-MALS data and further support that, if the samples are fresh, the KRAS/RGL1-RA complex exists as a 1:1 dimer and that the dissociation constant is nearly identical between wild-type and mutant G12V in KRAS (see Figure 8).

Discussion

Despite the RalGDS family emerging as important effectors of mutant RAS, the RalGEF

pathway has not been well characterized, with limited mechanistic and structural details of RAS-RalGEF interactions.[4] Among many RAS-stimulating GEFs, Kuriyan and co-workers have elegantly demonstrated mechanistic insights into the regulation of SOS and RASGRP1, two RAS-specific nucleotide exchange factors.[29–31] SOS is inactive unless RAS is bound to an allosteric site on the opposite side of the Cdc25-REM domain, which is blocked by the Dbl homology and pleckstrin homology (PH) domains of SOS.[32–33] Phosphatidylinositol-4,5-bisphosphate (PIP_2) binding and electrostatic interactions between the histone domain and the membrane reorient SOS to increase the accessibility of the RAS binding sites. In an analogous but distinct manner, the RAS-binding site of RASGRP1 is blocked by an interdomain linker and dimerization blocks the membrane interaction surface.[30] Calcium binding to the regulatory module of RASGRP1 and membrane docking disrupt the dimerization interface and reorient the inhibitory linker, releasing it from the RAS-binding site.

Interestingly, there is also a second Ral-specific GEF family - the RalGPS family - including RalGPS1 and RalGPS2,[15,21] which have an N-terminal Cdc25-like GEF domain but, unlike the RalGDS family, the RalGPS family members lack RA domains or RBDs, hence they are not directly activated by RAS. Instead, RalGPS1 and RalGPS2 have a C-terminal PH domain. The PH domain of RalGPS2 preferentially binds PIP_2 and is necessary for membrane localization. A central PxxP motif in the RalGPS members binds SH3-domain containing proteins such as Grb2 and PLCγ. The PH domain is required for in vivo GEF activity and the SH3 domain interactions contribute to RalGPS function, suggesting that the function of this RalGEF family is activated by localization and may involve additional allosteric regulation via these accessary domains. Based on these previous observations, it is most likely that the RalGDS family is regulated by molecular interactions that facilitate its translocation from the cytoplasm to the plasma membrane. However, as RGL1 and RGL2 do not possess such accessory modules in the sequence and consist of REM, Cdc25, and RA domains only (Figure 1(a)), their regulatory mechanisms may be simpler. Translocation to the membrane, mediated by KRAS binding to the RA domain, plays a key role in RGL1/RGL2 activation, but it remains unknown whether autoinhibitory interactions or allostery are involved.

To pave the way towards our full mechanistic understanding of how RGL1 is regulated by KRAS and other factors, we determined the structures of

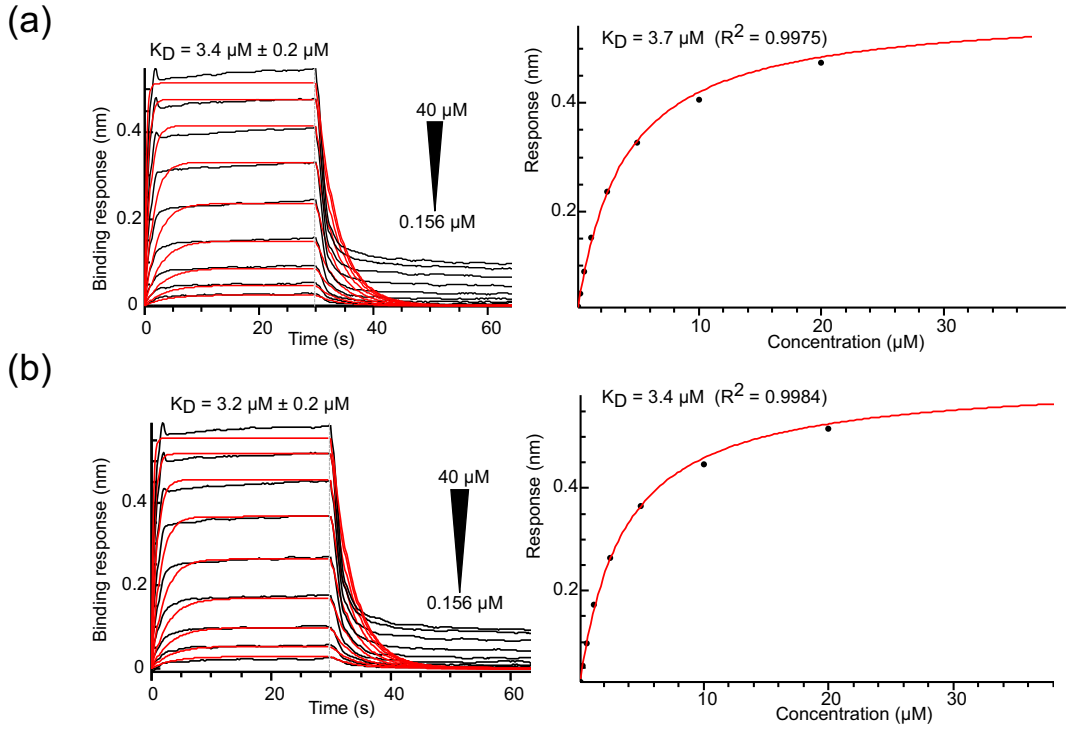

Figure 8. Biolayer interferometry analyses of $KRAS^{WT}$ and $KRAS^{G12V}$ interactions with RGL1-RA. Biolayer interferometry sensograms representing interactions between immobilized GST-RGL1-RA and GTPγS bound wild-type KRAS (a) and G12V (b). The ranges of KRAS concentrations are indicated beside each sensorgram. Left: sensorgram curves are shown in black with the fitted curves in red and the ***Kd*** values determined by kinetic analyses displayed above. Right: BLI response at equilibrium versus KRAS concentration with ***Kd*** values determined by steady-state analysis.

$KRAS^{WT}$ and $KRAS^{G12V}$ in complex with RGL1-RA. The structure of $KRAS^{WT}$-GTPγS bound to RGL1-RA is similar to that of the activated, free form of KRAS-GMPPMP (PDB code 6GOD) with a root-mean-square deviation (RMSD) of 0.47 Å for 157 atoms.[34] Switch I and switch II show slight differences between the two structures. Although the hypervariable region is present in this construct, no electron density was observed for residues C-terminal to 169, which is attributed to flexibility of the HVR. Currently, the only crystal structure where all residues in KRAS are observed, is a KRAS-PDEδ complex (PDB code 5TAR), in which a helical structure of the HVR structure is apparently stabilized by the interaction with PDEδ.[35]

The structure of RGL1-RA bound to KRAS is generally similar to the crystal structure of the free form of its homolog RalGDS (PDB code: 1LXD) with a RMSD of 0.56 Å for 77 atoms.[19] The major differences involve residues 690–699, a loop region between β-strands 1 and 2, and 724–727, a loop region between α-helix 1 and β-strand 3. These differences appear to arise from rearrangements associated with the RAS-binding interface. However, an NMR-derived solution structure of mouse RGL1-RA (PDB code: 1EF5) is more structurally divergent from our crystal structure, with a RMSD of 3.94 Å for 85 atoms,[10] than the RalGDS crystal structure. The sequences of human RGL1-RA and mouse RGL1-RA are almost (96.7%) identical, thus the structural divergence is more likely a result of the determination of their structures by different methods. The solution NMR structure may represent an average of distinct states found in solution, while crystallization captured a single state. Additionally, the overall structure of the complex shows high similarity to that of HRAS-RalGDS (RMSD 0.44 Å, 218 atoms), with small differences between the structure of RalGDS and RGL1.

To our surprise, the present study revealed an extended conformation of the C-terminus of RGL1-RA in the $KRAS^{G12V}$/RGL1-RA crystal. The electron density present in this region (SI Figure 1) of the $KRAS^{G12V}$/RGL1 crystal structure can only be fit by a model in which RGL1-RA exists as a domain-swapped dimer (SI Figure 2). The loop region consisting of residues 758–761 acts as a hinge, opening to allow the C-terminal beta-strand (residues 761–767) to domain-swap with another RGL1-RA molecule. The domain-swapped regions had an interface area of 3875 $Å^2$, whilst the canonical interface buried 1138 $Å^2$ and the additional $KRAS^{G12V}$/RGL1 crystal contacts involved 901 $Å^2$. Thus, the heterotetrameric assembly observed in the crystal is stabilized mainly by the domain-swapped RGL1-RA strand. However, our observations of the $KRAS^{G12V}$/RGL1 complex by NMR did not provide strong evidence for the existence of stable heterotetramers in solution. The electron density of $KRAS^{WT}$/RGL1-RA provided no indication that the domain-swapping observed in the $KRAS^{G12V}$/RGL1-RA crystal was present in the wild-type complex. Despite the differences associated with domain-swapping of RGL1-RA, the KRAS WT/G12V complexes share remarkable structural similarity with a RMSD of 0.34 Å for 211 atoms. As would be expected, the major difference arises from residues 758–768, which are involved in the tetramerization via domain-swapping. There are minor differences at residues 736–742 and 724–727 which appear to be adjustments to facilitate the C-terminal beta-strand of the other RGL1-RA molecule involved in the domain-swapped dimer.

Domain swapped structures have not been previously reported for RAs or the structurally similar RBDs. RGL1-RA domain-swapping requires the detachment of the β-5 strand, the central strand in a 5-stranded β-sheet, which would involve transient disruption of 10 backbone hydrogen bonds and extraction of 5 hydrophobic side chains (V759, F761, F763, I764, L765) from the domain's hydrophobic core. This indicates the transition to assemble or disassemble a RGL1-RA domain-swapped dimer would need to overcome a very high activation energy. Domain swapping of a central beta-strand in the protein SUC1,[36] proceeds via a transition state that involves extensive unfolding and occurs on a time scale of months. Such slow exchange would be consistent with the SEC-MALS analyses of KRAS:RGL1 samples, by which no heterotetramer was detected in freshly prepared samples, but after several months a significant portion of the KRAS that remained complexed with RGL1 (presumably the fraction that persisted in the GTPγS-bound state) eluted as a heterotetramer. The SEC-MALS results support the ability of KRAS-RGL1 to form heterotetramers in solution, although the time required casts doubt on their physiological relevance. At present, we do not know the significance of this extremely slow tetramerization of the KRAS/RGL1-RA complex, which was observed only in the $KRAS^{G12V}$ crystal, but it is conceivable that macromolecular crowding and membrane association of the KRAS-RGL1 complex may promote heterotetramerization. Indeed, the first structure of the luminal domain of the ER membrane protein SARAF revealed a domain-swapped dimer, and FRET studies support domain-swapped dimerization of the full-length protein anchored in the ER membrane, while dimerization of the luminal domain in solution was just above the detection limit of equilibrium analytical ultracentrifugation.[37] Further studies are necessary to understand the RalGDS family and their regulation.

Our careful comparison of the structures of the KRAS/RGL1-RA complexes with those of other RAS-bound effector complexes identified distinct features in the current structures, while sharing the well-established topological similarities with other RAS effectors. Our findings reveal the manner in which the RGL1-RA domain docks onto

the KRAS structure. First, the distance between α1 helix of RGL1-RA and α1 of KRAS is significantly larger (21.7 Å) compared to that between RAFs and RAS (15.2–17.7 Å). The RAS/RalGDS-family complexes show relatively large $\alpha1^{RAS}/\alpha1^{Effector}$ distances, together forming a cluster in the plot of $\alpha1^{RAS}/\alpha1^{Effector}$ distances and angles while RAS/RAF complexes form another distinct cluster in the map (Figure 4). The angle between the two intermolecular α1 helices is relatively similar between RGL1-RA and RAF RBDs (74.0 and 71.4°, respectively), while this angle clearly distinguishes some outliers such as PI3K (64.2°), Byr2 (65.9°), PLCε (83.6°), and RASSF5 (85.4°) from the RalGDS (including RGL1-RA) and RAF clusters. These differences are likely dictated by the differences in amino acid sequence especially in the intermolecular interfaces. Indeed, our analysis using the contact maps clearly demonstrates the differences in domain packing between RAS and RBDs/RAs. We identified RA-specific contact sites involving the loop region between β1 and β2 of the effector and α1 of RAS as well as RBD specific contact sites involving the α1 helix of the effector and α1 helix/switch I region of RAS, and the loop region between β1 and β2 of the effector and the β2 strand of RAS (Figure 5). For the KRAS/RGL1-RA complexes this RA-specific contact is present in the crystal structures between Gln25 (KRAS) and Asn695 (RGL1-RA). While the core interaction between RAS switch I and β2 of RAs and RBDs is common to both classes, their distinct peripheral interactions with RAS suggest that inhibitors that target transient pockets surrounding the switch regions, or inhibitors that exert allosteric effects on these regions, could have differential impact on the binding of RAs versus RBDs. In summary, the present structural analysis revealed compelling structural differences among our KRAS/RGL1-RA structures and all other RAS/effector complexes reported so far, highlighting the significance of the diversity in the molecular recognition process involving multiple RAS effectors. Furthermore, we propose that measuring the $\alpha1^{KRAS}/\alpha1^{Effector}$ distance and angle offers a useful tool to classify the RAS/effector complexes into different subgroups and that the contact map provides an easy pictorial tool to identify structural signatures for the different subgroups of RAS-effector interactions.

Experimental procedures

Protein preparation

Full length human $KRAS4B^{WT/G12V}$ (residues 1–185, C118S, lacking the farnesylated and methylated C185 at the C-terminus), and RGL1-RA (residues 681–773) were expressed as His-tagged and GST-tagged proteins, respectively in Escherichia coli (BL21 DE3 Codon+) and purified as reported previously.[38–39] To produce uniformly labelled proteins, E. coli was grown in minimal M9 media supplemented with $^{15}NH_4Cl$ with or without ^{13}C-glucose.

In brief, KRAS and RGL1-RA expression was induced with 0.25 mM isopropyl-1-thio-β-D galactopyranoside at 18 °C overnight. Proteins were purified using Ni-NTA or Glutathione Sepharose resin and the tags were removed by thrombin cleavage. Proteins were then further purified by size exclusion chromatography using Superdex-75 columns. Purified KRAS was loaded with GTPγS in the presence of EDTA and Calf intestinal alkaline phosphatase (CIP). Excess nucleotide, EDTA and CIP were removed by passage through a Superdex-75 column.

Biolayer interferometry

The affinity of $KRAS^{WT/G12V}$ to RGL1-RA was measured using an Octet RED-384 biolayer interferometry instrument as previously described.[40] Briefly, the assay was performed using 96-well plates at 25 °C with 100 rpm agitation in a buffer consisting of 20 mM HEPES, 100 mM NaCl, 5 mM $MgCl_2$, and 2 mM TCEP supplemented with 1% BSA and 0.005% Tween-20 to minimize non-specific binding. GST-tagged RGL1-RA was immobilized to anti-GST-conjugated biosensors (Sartorius FortéBio) which were then dipped into wells containing increasing concentrations of GTPγS-loaded $KRAS^{WT/G12V}$.

Crystallography

Crystals of $KRAS^{WT}$ (1–185) bound to RGL1-RA (681–773) were obtained by incubating a mixture of purified GTPγS-loaded $KRAS^{WT}$ (14 mg ml^{-1}) and RGL1-RA (28 mg ml^{-1}) (20 mM HEPES pH 7.4, 100 mM NaCl, 5 mM $MgCl_2$, 2 mM TCEP) against a crystallization solution (0.05 M Magnesium acetate tetrahydrate, 0.1 M MES (pH 6.5), 26% v/v PEG 400) by sitting drop vapor diffusion at 25 °C. Crystals were cryo-protected by addition of 20% glycerol to the crystallization buffer, then flash cooled in liquid nitrogen. Diffraction data was collected on the AMX beamline at the National Synchrotron Light Source II (Brookhaven National Laboratory, Upton, NY).

Crystals of $KRAS^{G12V}$ (1–185) bound to RGL1-RA (681–773) did not form in the same condition as the $KRAS^{WT}$ complex. Crystals were obtained by incubating purified GTPγS-loaded $KRAS^{G12V}$ (20 mg ml^{-1}) and RGL1-RA (20 mg ml^{-1}) (20 mM HEPES pH 7.4, 100 mM NaCl, 5 mM $MgCl_2$, 2 mM TCEP) against a crystallization solution (0.1 M BIS-TRIS (pH 5.5), 25% w/v PEG 3350) by sitting drop vapor diffusion at 25 °C. Crystals were cryo-protected by addition of 20% glycerol to the crystallization buffer, then flash cooled in liquid nitrogen. Diffraction data was collected on

Beamline 17-ID at the Advanced Photon Source (Argonne National Laboratory, Argonne, IL).

The structures were solved by molecular replacement in the program Phaser using the structure of HRAS complexed to RalGDS (1LFD) as a search model.[18,41] Multiple successive rounds of refinement using PHENIX accompanied by manual model building with Coot was used to generate the final models.[42–43] Figures were prepared using PyMOL and Ligplot.[44–45] Data collection and refinement statistics are shown in Table S1. Interface areas of the assemblies were calculated using PISA.[46]

NMR spectroscopy

NMR experiments were performed at 25 °C on a Bruker ultra-shield 800 MHz, NEO spectrometer equipped with a 5 mm triple-resonance TXO cold-probe, z-gradient, and on a Bruker Ascend 700 MHz, AVANCE III HD spectrometer equipped with a 5 mm triple-resonance TCI cold-probe with xyz-gradient. NMR samples were prepared in a buffer containing 20 mM HEPES (pH 7.4), 100 mM NaCl, 2 mM TCEP, 5 mM $MgCl_2$ and 10% D_2O. Spectra were processed with the NMRPipe software and analyzed using the NMRFAM-SPARKY program.[47–48]

RGL1 assignments were performed based on the HNCO, HNCOCA, HNCACB, CBCACONH, and 3D ^{1}H-^{15}N edited-NOESY-HSQC (90 ms mixing time) spectra, as well as ^{1}H-^{15}N HSQC spectra. Peaks were initially picked by the APES function in NMRFAM-SPARKY and then input into I-PINE for automated backbone assignment which was then verified by PINE-SPARKY.[49–51]

KRAS backbone amide assignments were transferred from KRAS-GTP (BMRB code: 28021). NMR chemical shift perturbation was visualized onto structures using UCSF Chimera.[52] Chemical shift perturbations were calculated using the formula $\Delta\delta NH.N(ppm)=\sqrt{([(\Delta H)]2 + [(\Delta N/5)]2)}$ and plotted against residue number using GraphPad 9.1.0.

Helical distances/angles and contact maps

Distances and angles between the α1 helix of RAS and the α1 helix of the effector in each complex were calculated within PyMOL using the helix_angle.py script provided by Robert L. Campbell under license (CC BY-NC-SA 4.0).[44] Distances were measured from the midpoint of the helices and angles were calculated between the helical vectors.

Contact maps were calculated and visualized using Python.[53] A binary matrix with the rows and columns representing the residues of either the effector or RAS was calculated and the residues were considered in contact if the α-carbon distance between the pair of residues was less than 12 Å.

CRediT authorship contribution statement

Ben J. Eves: Conceptualization, Methodology, Visualization, Investigation, Formal analysis, Validation, Writing – original draft, Writing – review & editing. **Teklab Gebregiworgis:** Conceptualization, Investigation, Writing – review & editing. **Geneviève M.C. Gasmi-Seabrook:** Investigation, Writing – review & editing. **Douglas A. Kuntz:** Formal analysis, Writing – review & editing. **Gilbert G. Privé:** Formal analysis, Writing – review & editing. **Christopher B. Marshall:** Conceptualization, Writing – review & editing, Funding acquisition. **Mitsuhiko Ikura:** Conceptualization, Writing – review & editing, Funding acquisition.

DATA AVAILABILITY

Coordinates for the $KRAS^{WT}$-RGL1 and $KRAS^{G12V}$-RGL1 crystal structures are deposited in the protein data bank (PDB) with accession codes: 7SCW and 7SCX, respectively.

Assigned resonances for RGL1-RA were deposited in the BMRB with access number: 51110.

Acknowledgments

Data was collected at the Advanced Photon Source (Argonne National Laboratory, Argonne, IL) and the National Synchrotron Light Source II (Brookhaven National Laboratory, Upton, NY).

Author contributions

B.J.E., T.G., C.B.M. and M.I. conceived the project. B.J.E purified proteins and prepared protein crystals. B.J.E solved and processed crystal structures with the assistance of D.A.K and G.G.P. B.J.E with G.M.C.G.-S. performed the NMR experiments and B.J.E analyzed the NMR data. B.J.E and T.G. performed and analyzed BLI and SEC-MALS experiments. B.J.E. wrote the manuscript with essential input and feedback from all other authors.

Funding and additional information

B.J.E. is the recipient of a George and Helen Vari Foundation Fellowship. This work was supported by funds from the Canadian Cancer Society Research Institute (703209), Princess Margaret Foundation, Canadian Institutes of Health Research (FDN-1542284). M.I. holds a Canada Research Chair in cancer structural biology. The Princess Margaret NMR facility is funded by the Canada Foundation for Innovation and the NMR Core Facility was supported by the Princess Margaret Cancer Foundation.

Conflict of interest

The authors declare that they have no conflicts of interest with the contents of this article.

Appendix A. Supplementary data

Supplementary data to this article can be found online at https://doi.org/10.1016/j.jmb.2022.167527.

Received 30 September 2021;
Accepted 1 March 2022;
Available online 4 March 2022

Keywords:
GTPase KRAS (KRAS);
cancer biology;
X-ray crystallography;
nuclear magnetic resonance (NMR);
structure

Abbreviations used:
RGL1, Ral Guanine Nucleotide Dissociation Stimulator Like 1; RA, RAS-association; SEC-MALS, size-exclusion chromatography combined with multi-angle light scattering; Ral, RAS-like; RalGEFs, Ral guanine nucleotide exchange factors; RalGDS, Ral guanine nucleotide dissociation stimulator; RGL1, RalGDS Like 1; REM, RAS exchange motif; TIPE2, Tumor necrosis factor alpha induced protein 8-like 2; RBDs, RAS-binding domains; HVR, hypervariable region; NMR, nuclear magnetic resonance; HSQC, heteronuclear single quantum coherence; GTPγS, guanosine 5′-O-[gamma-thio]triphosphate; SOS, Son of Sevenless; RASGRP1, RAS guanine nucleotide releasing protein 1; PH, pleckstrin homology; PIP_2, Phosphatidylinositol-4,5-bisphosphate; RMSD, root-mean-square deviation; IDR, intrinsically disordered region; CIP, Calf intestinal alkaline phosphatase

References

1. Prior, I.A., Hood, F.E., Hartley, J.L., (2020). The Frequency of Ras Mutations in Cancer. *Cancer Res.* **80**, 2969–2974.
2. Hanahan, D., Weinberg, R.A., (2011). Hallmarks of Cancer: The Next Generation. *Cell* **144**, 646–674.
3. Karnoub, A.E., Weinberg, R.A., (2008). Ras oncogenes: split personalities. *Nat. Rev. Mol. Cell Biol.* **9**, 517–531.
4. Neel, N.F., Martin, T.D., Stratford, J.K., Zand, T.P., Reiner, D.J., Der, C.J., (2011). The RalGEF-Ral Effector Signaling Network: The Road Less Traveled for Anti-Ras Drug Discovery. *Genes & Cancer.* **2**, 275–287.
5. Gus-Brautbar, Y., Johnson, D., Zhang, L., Sun, H., Wang, P., Zhang, S., Zhang, L., Chen, Y.H., (2012). The Anti-inflammatory TIPE2 Is an Inhibitor of the Oncogenic Ras. *Mol. Cell.* **45**, 610–618.
6. Shirakawa, R., Horiuchi, H., (2015). Ral GTPases: crucial mediators of exocytosis and tumourigenesis. *J. Biochem.* **157**, 285–299.
7. Nakhaeizadeh, H., Amin, E., Nakhaei-Rad, S., Dvorsky, R., Ahmadian, M.R., (2016). The RAS-Effector Interface: Isoform-Specific Differences in the Effector Binding Regions. *PLoS ONE* **11**, e0167145
8. Ponting, C.P., Benjamin, D.R., (1996). A novel family of Ras-binding domains. *Trends Biochem. Sci.* **21**, 422–425.
9. Zago, G., Veith, I., Singh, M.K., Fuhrmann, L., De Beco, S., Remorino, A., Takaoka, S., Palmeri, M., Berger, F., Brandon, N., El Marjou, A., Vincent-Salomon, A., Camonis, J., Coppey, M., Parrini, M.C., (2018). RalB directly triggers invasion downstream Ras by mobilizing the Wave complex. *eLife* **7**, e40474
10. Kigawa, T., Endo, M., Ito, Y., Shirouzu, M., Kikuchi, A., Yokoyama, S., (1998). Solution structure of the Ras-binding domain of RGL. *FEBS Lett.* **441**, 413–418.
11. Berns, A., (2008). Kras and Hras—what is the difference? *Nat. Genet.* **40**, 1149–1150.
12. Parker, J.A., Volmar, A.Y., Pavlopoulos, S., Mattos, C., (2018). K-Ras Populates Conformational States Differently from Its Isoform H-Ras and Oncogenic Mutant K-RasG12D. *Structure.* **26**, 810–820.e4.
13. Buhrman, G., O′Connor, C., Zerbe, B., Kearney, B. M., Napoleon, R., Kovrigina, E. A., Vajda, S., Kozakov, D., Kovrigin, E. L. & Mattos, C. (2011). Analysis of Binding Site Hot Spots on the Surface of Ras GTPase. *J. Mol. Biol.* **413**, 773–789.
14. Waters, A.M., Ozkan-Dagliyan, I., Vaseva, A.V., Fer, N., Strathern, L.A., Hobbs, G.A., Tessier-Cloutier, B., Gillette, W.K., Bagni, R., Whiteley, G.R., Hartley, J.L., McCormick, F., Cox, A.D., Houghton, P.J., Huntsman, D.G., Philips, M. R., Der, C.J., (2017). Evaluation of the selectivity and sensitivity of isoform- and mutation-specific RAS antibodies. *Sci. Signal.* **10**, eaao3332.
15. Gorfe, A.A., Grant, B.J., McCammon, J.A., (2008). Mapping the Nucleotide and Isoform-Dependent Structural and Dynamical Features of Ras Proteins. *Structure.* **16**, 885–896.
16. Johnson, C.W., Reid, D., Parker, J.A., Salter, S., Knihtila, R., Kuzmic, P., Mattos, C., (2017). The small GTPases K-Ras, N-Ras, and H-Ras have distinct biochemical properties determined by allosteric effects. *J. Biol. Chem.* **292**, 12981–12993.
17. Guin, S., Theodorescu, D., (2015). The RAS-RAL axis in cancer: evidence for mutation-specific selectivity in non-small cell lung cancer. *Acta Pharmacol. Sin.* **36**, 291–297.
18. Huang, L., Hofer, F., Martin, G.S., Kim, S.-H., (1998). Structural basis for the interaction of Ras with RalGDS. *Nat. Struct. Mol. Biol.* **5**, 422–426.
19. Huang, L., Weng, X., Hofer, F., Martin, G.S., Kirn, S.-H., (1997). Three-dimensional structure of the Ras-interacting domain of RalGDS. *Nat. Struct. Mol. Biol.* **4**, 609–615.
20. Nassar, N., Horn, G., Herrmann, C.A., Scherer, A., McCormick, F., Wittinghofer, A., (1995). The 2.2 Å crystal structure of the Ras-binding domain of the serine/threonine kinase c-Raf1 in complex with RapIA and a GTP analogue. *Nature* **375**, 554–560.

21. Fetics, S.K., Guterres, H., Kearney, B.M., Buhrman, G., Ma, B., Nussinov, R., Mattos, C., (2015). Allosteric Effects of the Oncogenic RasQ61L Mutant on Raf-RBD. *Structure.* **23**, 505–516.
22. Ren, J., Wen, L., Gao, X., Jin, C., Xue, Y., Yao, X., (2009). DOG 1.0: illustrator of protein domain structures. *Cell Res.* **19**, 271–273.
23. Wohlgemuth, S., Kiel, C., Krämer, A., Serrano, L., Wittinghofer, F., Herrmann, C., (2005). Recognizing and Defining True Ras Binding Domains I: Biochemical Analysis. *J. Mol. Biol.* **348**, 741–758.
24. Ikura, M., Kay, L.E., Bax, A., (1990). A novel approach for sequential assignment of 1H, 13C, and 15N spectra of proteins: heteronuclear triple-resonance three-dimensional NMR spectroscopy. Application to calmodulin. *Biochemistry.* **29**, 4659–4667.
25. Laskowski, R.A., Jabłońska, J., Pravda, L., Vařeková, R.S., Thornton, J.M., (2018). PDBsum: Structural summaries of PDB entries. *Protein Sci.* **27**, 129–134.
26. Håkansson, M., Svensson, A., Fast, J., Linse, S., (2001). An extended hydrophobic core induces EF-hand swapping. *Protein Sci.* **10**, 927–933.
27. Rousseau, F., Schymkowitz, J.W.H., Wilkinson, H.R., Itzhaki, L.S., (2001). Three-dimensional domain swapping in p13suc1 occurs in the unfolded state and is controlled by conserved proline residues. *PNAS* **98**, 5596–5601.
28. Schlunegger, M., Bennett, M. & Eisenberg, D. (1997). Oligomer Formation By 3D Domain Swapping: A Model For Protein Assembly And Misassembly. pp. 61–122. *In*: *Advances in Protein Chemistry*, Elsevier.
29. Boriack-Sjodin, P.A., Margarit, S.M., Bar-Sagi, D., Kuriyan, J., (1998). The structural basis of the activation of Ras by Sos. *Nature* **394**, 337–343.
30. Iwig, J.S., Vercoulen, Y., Das, R., Barros, T., Limnander, A., Che, Y., Pelton, J.G., Wemmer, D.E., Roose, J.P., Kuriyan, J., (2013). Structural analysis of autoinhibition in the Ras-specific exchange factor RasGRP1. *eLife* **2**, e00813
31. Margarit, S.M., Sondermann, H., Hall, B.E., Nagar, B., Hoelz, A., Pirruccello, M., Bar-Sagi, D., Kuriyan, J., (2003). Structural Evidence for Feedback Activation by Ras·GTP of the Ras-Specific Nucleotide Exchange Factor SOS. *Cell* **112**, 685–695.
32. Gureasko, J., Kuchment, O., Makino, D.L., Sondermann, H., Bar-Sagi, D., Kuriyan, J., (2010). Role of the histone domain in the autoinhibition and activation of the Ras activator Son of Sevenless. *Proc. Natl. Acad. Sci. U.S.A.* **107**, 3430–3435.
33. Sondermann, H., Soisson, S.M., Boykevisch, S., Yang, S.-S., Bar-Sagi, D., Kuriyan, J., (2004). Structural analysis of autoinhibition in the Ras activator Son of sevenless. *Cell* **119**, 393–405.
34. Cruz-Migoni, A., Canning, P., Quevedo, C.E., Bataille, C.J. R., Bery, N., Miller, A., Russell, A.J., Phillips, S.E.V., Carr, S.B., Rabbitts, T.H., (2019). Structure-based development of new RAS-effector inhibitors from a combination of active and inactive RAS-binding compounds. *Proc. Natl. Acad. Sci. U.S.A.* **116**, 2545–2550.
35. Dharmaiah, S., Bindu, L., Tran, T.H., Gillette, W.K., Frank, P.H., Ghirlando, R., Nissley, D.V., Esposito, D., McCormick, Stephen, A.G., Simanshu, D.K., (2016). Structural basis of recognition of farnesylated and methylated KRAS4b by PDEδ. *Proc. Natl. Acad. Sci. U.S. A.* **113**, E6766–E6775.
36. Rousseau, F., Schymkowitz, J.W.H., Itzhaki, L.S., (2003). The Unfolding Story of Three-Dimensional Domain Swapping. *Structure.* **11**, 243–251.
37. Kimberlin, C.R., Meshcheriakova, A., Palty, R., Raveh, A., Karbat, I., Reuveny, E., Minor, D.L., (2019). SARAF Luminal Domain Structure Reveals a Novel Domain-Swapped β-Sandwich Fold Important for SOCE Modulation. *J. Mol. Biol.* **431**, 2869–2883.
38. Fang, Z., Lee, K.-Y., Huo, K.-G., Gasmi-Seabrook, G., Zheng, L., Moghal, N., Tsao, M.-S., Ikura, M., Marshall, C. B., (2020). Multivalent assembly of KRAS with the RAS-binding and cysteine-rich domains of CRAF on the membrane. *Proc. Natl. Acad. Sci. U.S.A.* **117**, 12101–12108.
39. Smith, M.J., Ikura, M., (2014). Integrated RAS signaling defined by parallel NMR detection of effectors and regulators. *Nat. Chem. Biol.* **10**, 223–230.
40. Kano, Y., Gebregiworgis, T., Marshall, C.B., Radulovich, N., Poon, B.P.K., St-Germain, J., Cook, J.D., Valencia-Sama, I., Grant, B.M.M., Herrera, S.G., Miao, J., Raught, B., Irwin, M.S., Lee, J.E., Yeh, J.J., Zhang, Z.-Y., Tsao, M.-S., Ikura, M., Ohh, M., (2019). Tyrosyl phosphorylation of KRAS stalls GTPase cycle via alteration of switch I and II conformation. *Nat. Commun.* **10**, 224.
41. Bunkóczi, G., Echols, N., McCoy, A.J., Oeffner, R.D., Adams, P.D., Read, R.J., (2013). *Phaser.MRage* : automated molecular replacement. *Acta Crystallogr. D Biol. Crystallogr.* **69**, 2276–2286.
42. Emsley, P., Cowtan, K., (2004). *Coot* : model-building tools for molecular graphics. *Acta Crystallogr. D Biol. Crystallogr.* **60**, 2126–2132.
43. Liebschner, D., Afonine, P.V., Baker, M.L., Bunkóczi, G., Chen, V.B., Croll, T.I., Hintze, B., Hung, L.-W., Jain, S., McCoy, A.J., Moriarty, N.W., Oeffner, R.D., Poon, B.K., Prisant, M.G., Read, R.J., Richardson, J.S., Richardson, D. C., Sammito, M.D., Sobolev, O.V., Stockwell, D.H., Terwilliger, T.C., Urzhumtsev, A.G., Videau, L.L., Williams, C.J., Adams, P.D., (2019). Macromolecular structure determination using X-rays, neutrons and electrons: recent developments in *Phenix. Acta Crystallogr. D Struct. Biol.* **75**, 861–877.
44. Schrödinger, LLC The PyMOL Molecular Graphics System, Version 2.2.3.
45. Wallace, A.C., Laskowski, R.A., Thornton, J.M., (1995). LIGPLOT: a program to generate schematic diagrams of protein-ligand interactions. *Protein Eng. Des. Sel.* **8**, 127–134.
46. Krissinel, E., Henrick, K., (2007). Inference of Macromolecular Assemblies from Crystalline State. *J. Mol. Biol.* **372**, 774–797.
47. Delaglio, F., Grzesiek, S., Vuister, GeertenW., Zhu, G., Pfeifer, J., Bax, A., (1995). NMRPipe: A multidimensional spectral processing system based on UNIX pipes. *J Biomol. NMR.* **6**, 277–293.
48. Lee, W., Tonelli, M., Markley, J.L., (2015). NMRFAM-SPARKY: enhanced software for biomolecular NMR spectroscopy. *Bioinformatics* **31**, 1325–1327.

49. Lee, W., Bahrami, A., Dashti, H.T., Eghbalnia, H.R., Tonelli, M., Westler, W.M., Markley, J.L., (2019). I-PINE web server: an integrative probabilistic NMR assignment system for proteins. *J. Biomol. NMR.* **73**, 213–222.
50. Lee, W., Markley, J.L., (2018). PINE-SPARKY.2 for automated NMR-based protein structure research. *Bioinformatics* **34**, 1586–1588.
51. Shin, J., Lee, W., Lee, W., (2008). Structural proteomics by NMR spectroscopy. *Expert Rev. Proteom.* **5**, 589–601.
52. Pettersen, E.F., Goddard, T.D., Huang, C.C., Couch, G.S., Greenblatt, D.M., Meng, E.C., Ferrin, T.E., (2004). UCSF Chimera - A visualization system for exploratory research and analysis. *J. Comput. Chem.* **25**, 1605–1612.
53. Van Rossum, G., Drake, F.L., (2009). Python 3 Reference Manual. CreateSpace, Scotts Valley, CA.